Journal of Applied Electrochemistry **31**: 293–300, 2001.

Influence of iron addition on the microstructure and the electrochemical corrosion of Al–Zn–Mg alloys

A.V. BENEDETTI[1], P.L. CABOT[2], J.A. GARRIDO[2] and A.H. MOREIRA[3]
[1]*Departamento de Físico-Química, Instituto de Química, UNESP, Caixa Postal 355, 14.801-970, Araraquara, SP, Brazil*
[2]*LCTEM, Departament de Química Física, Facultat de Química, Universitat de Barcelona, Martí i Franquès, 1, 08028, Barcelona, Spain*
[3]*Departamento de Química Analítica e Físico-Química, UFC, Campus do Pici, Bloco 940, 60.451-970, Fortaleza, CE, Brazil*

Received 26 August 1999; accepted in revised form 30 May 2000

Key words: aluminium-based alloys, corrosion, heat treatment

Abstract

The effect of Fe addition on the microstructural properties and the corrosion resistance of Al–Zn–Mg alloys submitted to different heat treatments (cast, annealed and aged), has been studied in chloride solutions using optical microscopy (OM), scanning electron microscopy (SEM), transmission electron microscopy (TEM), energy-dispersive X-ray (EDX), cyclic polarization (CP) and open circuit potential (o.c.p.) measurements. The presence of 0.3% Fe in the alloy limited the growth of the $MgZn_2$ precipitates, both in the annealed and in the quenched specimens. No effect of Cr on the grain size in the presence of Fe was found because of the accumulation of Cr in the Fe-rich particles. Fe in the Al–Zn–Mg alloys also made them more susceptible to pitting. Pitting occurred mainly near the Fe-rich particles both, under o.c.p. conditions in O_2-saturated solutions and during the CP.

1. Introduction

Aluminium-based alloys have wide application as structural materials and in the aircraft industry due to their low density, hardness and high corrosion resistance, but their use is limited by different forms of corrosion such as pitting, intergranular corrosion, stress corrosion cracking (SCC) or exfoliation corrosion [1–7].

Al–(4.9–5.2%)Zn–(1.6–1.8%)Mg alloys are susceptible to SCC under certain conditions [1, 2, 7–13]. Mankowski et al. [14] have examined different criteria to evaluate the susceptibility to SCC of Al–Zn–Mg alloys in chloride-containing aqueous solutions on the basis of dynamic straining data. They concluded that fracture energy and elongation at fracture ratios are more convenient criteria than maximum load ratio and area reduction to evaluate the SCC resistance of these Al alloys. Some work has shown that addition of 0.15–0.29% copper and 0.15–0.25% chromium increased their SCC resistance [10].

The microstructure and electrochemical behaviour of Al–5%Zn–1.7%Mg–0.23%Cu (alloy H), Al–5%Zn–1.7%Mg–0.23%Cu–0.053%Nb (alloy J), Al–5%Zn–1.7%Mg–0.24%Cu–0.14%Cr (alloy L) and Al–5%Zn–1.7%Mg–0.24%Cu–0.14%Cr–0.053%Nb (alloy O), submitted to different heat treatments (A: annealed; ST: cold-rolled; F: quenched; B: quenched and aged and C: quenched in two steps and aged), were previously studied in chloride-containing solutions by means of OM, SEM, TEM, EDX and o.c.p. measurements [15–17], CP [18] and electrochemical impedance spectroscopy [19, 20]. Both Nb and Cr additions diminished the grain size of the Al–Zn–Mg alloy, Cr having a greater effect than Nb [15, 16]. On the other hand, the heat treatment modified the distribution and size of the $MgZn_2$ precipitates along the grains. Alloys submitted to treatment ST showed elongated grains oriented in the rolling direction, while polyhedric grains were observed for those submitted to treatments A, B, C and F. $MgZn_2$ precipitates were much bigger in alloys submitted to treatments ST and A (0.2–0.4 μm in length) than those observed for treatments B and C ($\sim$0.02 μm in length). No $MgZn_2$ precipitates were observed for treatment F. For treatments ST, A, B and C, the $MgZn_2$ precipitates were distributed both at the grain boundaries (GBs) and in the grain bodies. Addition of Nb slightly shifted the corrosion, pitting and repassivation potentials to more positive values, whereas a larger shift in the same direction was observed upon Cr addition [17, 18].

Many studies of microstructure, mechanical properties and electrochemical behaviour of the Al–Zn–Mg alloys can be found in the literature. However, most of the used alloys were prepared from high purity aluminium. It is well known that commercial Al contains Fe

impurities about 0.3–0.7%. These amounts reduce the electrochemical stability in corrosive environments and most of the mechanical properties of Al [1]. Iron has a very low solubility in aluminium, 0.004% Fe at 400 °C, usually causing the formation of intermetallic compounds such as $FeAl_3$ (a phase in equilibrium with the Al matrix) and, in some cases, $FeAl_6$ (which is not in equilibrium with the Al matrix) [21–23]. These intermetallics accelerate the aluminium corrosion [24]. As Fe-rich particles are cathodic with respect to the Al matrix, oxygen is reduced on the intermetallic phase and pitting is initiated in the aluminium alloy region around it.

The main effect of Fe on wrought Al alloys is a more or less pronounced deterioration of most of their properties [1]. The corrosion resistance of the 1xxx series decreases when its iron content is increased. The surface of the small iron-rich particles are covered by an oxide film thinner than that covering the exposed areas of the aluminium solid solution. Corrosion may be initiated earlier and progress more rapidly around these particles. The number and size of corrosion sites are proportional to the exposed area of the iron-rich particles relative to the overall exposed alloy area [25]. The intermetallics formed in Al–Zn–Mg alloys are also $FeAl_3$ when the alloys are slowly cooled or annealed, and $FeAl_6$, when they are quenched [1]. However, the effect of heat treatment on the type and distribution of these intermetallic compounds are not known. The effect of these precipitates in the corrosion mechanism of Al–Zn–Mg alloys has also not been studied. In this work, two different Al–4.3%Zn–1.9%Mg alloys, only one containing 0.14% Cr and both containing about 0.3% Fe, have been prepared and submitted to heat treatments A, B and ST. The effect of Fe on the microstructure and the susceptibility to localized corrosion of these alloys has been studied using OM, SEM, TEM, EDX, CP and o.c.p. measurements.

2. Experimental details

2.1. *Sample preparation and analyses*

Two Al–Zn–Mg alloys were prepared by mixing melts of Al–Zn and Al–Mg alloys with commercial Al, the first one containing Al, Zn, Mg and Cu (alloy 1), and the second Al, Zn, Mg, Cu and Cr (alloy 2). Melting of the elements was performed in an O_2-free Inductotherm oven at 1000 °C for 10 min. The results of inductively coupled plasma (ICP) analyses of the alloys are given in Table 1. The compositions of alloys 1 and 2 were close to those of H and L given in [17], respectively, but alloys H and L did not contain Fe.

The iron present in both samples was not deliberately introduced, but came from the commercial Al used for the alloy preparation. The same occurred with Cu in sample 1 and with Si in both samples. Conversely, Cu and Cr were deliberately introduced in alloy 2. The Fe content was not the same because the two alloys were prepared from two different pieces of commercial Al.

Table 1. Composition (in wt %) of Al–Zn–Mg–Cu–Fe alloys

Sample	Zn	Mg	Cu	Cr	Fe	Si
1	4.40	1.91	0.013	–	0.31	0.06
2	4.20	1.85	0.20	0.14	0.25	0.06

After preparation, the alloys were rolled and cut into thin ingots 3.0 cm × 1.0 cm × 0.2 cm. Some pieces were annealed at 480 °C for 24 h with slow cooling for 48 h down to room temperature (heat treatment A, samples 1A and 2A). Other pieces were first submitted to heat treatment A and were then heated at 480 °C for 1 h, quenched in water at 10 °C, held at room temperature for 8 h and subsequently, heated at 135 °C for 24 h (heat treatment B, samples 1B and 2B). Heat treatment B was an artificial age hardening. The pieces with no heat treatment were named ST (samples 1ST and 2ST).

2.2. *Microscopic examination*

The alloys were examined by OM (Zeiss-Axiovert 405M metallographic microscope), TEM (CM-200-Philips and CM-30-Philips), SEM (Stereoscan-120) and EDX (Link Systems).

Before the OM observation the samples were polished to 1 μm finish (using diamond spray), cleaned with ethanol in an ultrasonic bath and etched using Keller's reagent [26]. Some polished samples were also examined by SEM and EDX. TEM samples were prepared by cutting them to discs 3 mm in diameter. Both sides of the discs were polished up to 0.3 mm in thickness and they were then electrolytically polished using a Tenupol-3 Struers in 25% v/v HNO_3-methanol solution (7.5 V and 0.05 mA). The electrolytic polishing was automatically stopped when a small hole appeared in the disc.

2.3. *Electrochemical experiments*

To obtain the working electrodes, cylinders 3 mm in diameter were cut from the thin ingots previously prepared (the section exposed to the solution was 0.71 cm^2). Prior to the electrochemical tests, they were encapsulated in epoxy resin, polished using diamond paste up to a 1 μm finish and cleaned with ethanol in an ultrasonic bath. The electrochemical experiments were carried out in a conventional three-electrode cell at (25.0 ± 0.1) °C. The reference and auxiliary electrodes were a SCE, connected via a Luggin capillary, and a platinum wire, respectively. All the potentials given in this work are referred to the SCE.

The electrochemical experiments were performed using a PAR 273A potentiostat and the M342C corrosion software. The test solutions were prepared from Merck p.a. NaCl and Millipore Milli-Q quality water. The o.c.p. measurements were performed in O_2-saturated (1 atm) 0.1 M NaCl and also in 1 M NaCl + 9 ml

of 30% H_2O_2 per litre (ASTM G 69–81) Standard Practice [27]). The CP experiments were conducted in 0.1 M NaCl under deaerated conditions and also after 3 h of immersion in the O_2-saturated solutions. Deaeration was performed by Ar bubbling for 3 h through a vigorously stirred solution. Argon was circulating over the electrolyte during the experiments with deaerated solutions. The specimens were examined by SEM and EDX before and after these tests.

3. Results and discussion

3.1. *Microstructure of the alloys*

OM observations of the polished and etched alloys were performed to study the effect of composition and heat treatment on the form and size of the grains. Figure 1 shows micrographs obtained for alloy 1ST and 2B. Specimens 1ST and 2ST presented elongated grains, their GBs being less apparent than those of A and B because of rolling. Previous studies showed that the addition of 0.14% Cr to Al–Zn–Mg alloys without Fe caused a decrease of the mean grain size of the alloys for all heat treatments applied [15, 16]. However, this was not observed for Al–Zn–Mg alloys with 0.3% Fe. Alloys without Cr (1A and 1B) and with Cr (2A and 2B) presented the same form of the grains and the same mean grain size.

SEM observation of the polished Al–Zn–Mg alloys showed the existence of small particles with atomic weight greater than that of the matrix. EDX microanalyses of these particles showed the presence of Fe and Al, probably $FeAl_3$, the most stable compound formed between Al and Fe in these conditions [1, 24]. These particles were present in alloys 1 and 2 and their size did not depend on heat treatment.

Figure 2 shows SEM micrographs obtained for specimens 1 and 2 submitted to different heat treatments. $MgZn_2$ precipitates were not observed by SEM for any heat treatment, while for Al–Zn–Mg alloys without Fe and similar composition in Zn and Mg, a large amount of $MgZn_2$ precipitates in the GBs of the alloys submitted to heat treatment A and ST were found [16, 17]. This indicated that Fe limited the growth of $MgZn_2$.

SEM observations of the specimens after Keller's etch showed that the Fe-rich particles were localized at the GBs and in the inner part of the grains. However, the quantity of intergranular particles was greater than that of the intragranular ones. The latter were also smaller than the former (Figure 3). The size and distribution of Fe-rich intermetallics were not found to be dependent on the alloy composition and heat treatment (Figure 2).

As found previously [16], OM and SEM were not sufficient to observe very small $MgZn_2$ particles and, accordingly, the alloys were examined by TEM. Figure 4 shows TEM images of alloy 2B, in which a large quantity of small precipitates in the GBs and in the

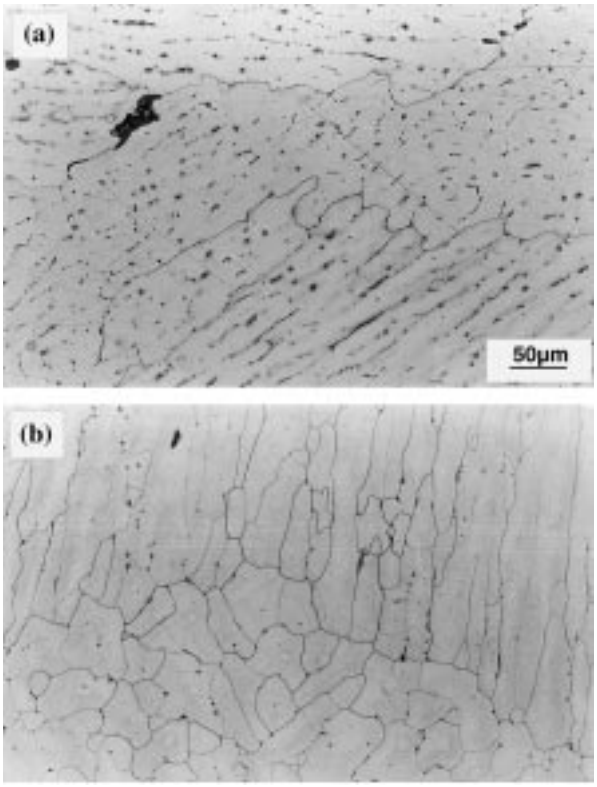

Fig. 1. Alloys 1ST (a) and 2B (b), etched with Keller's reagent.

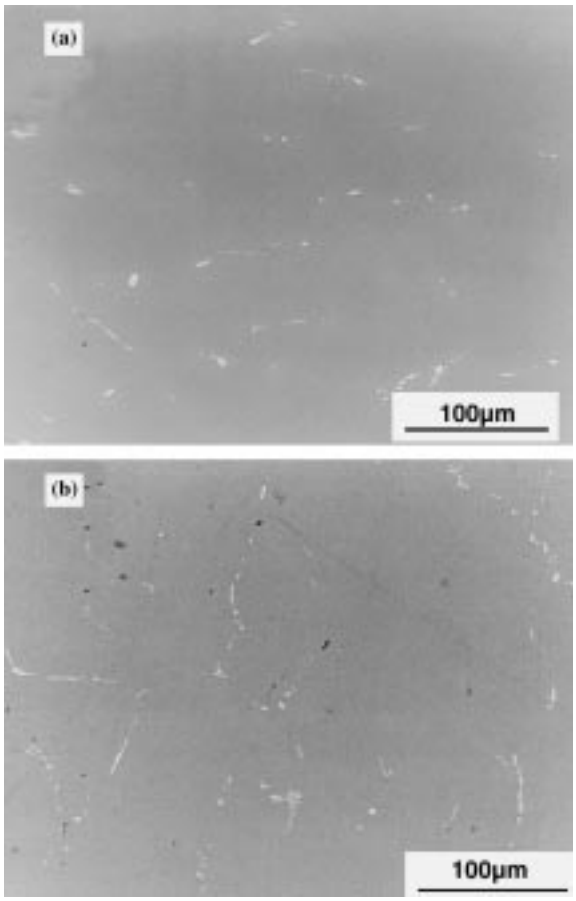

Fig. 2. SEM images of polished specimens: (a) 2ST and (b) 1B.

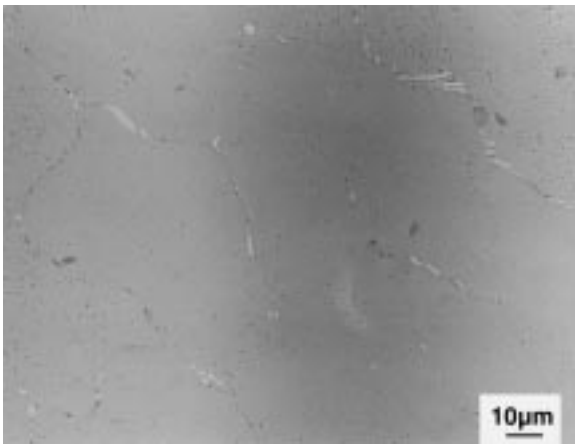

Fig. 3. SEM image of sample 1A, etched with Keller's reagent.

grain bodies is observed. The EDX microanalyses indicated the presence of Mg and Zn together with Al and Cr; it was assumed that they were $MgZn_2$ particles. The large Al peak in the EDX microanalyses of the $MgZn_2$ particles can be explained by the small size of the particles in relation to the electron beam. These precipitates were very similar to, but smaller than, those of $MgZn_2$ found for Al–Zn–Mg alloys without Fe [16, 17]. This was in agreement with the SEM observations, indicating again that Fe limited the growth of $MgZn_2$ precipitates. In addition, bigger Fe-rich particles localized at the GBs and in the inner part of the grains were also observed. Chromium was also detected in them by EDX. According to the Al–Cr and Cr–Fe binary equilibrium diagrams, Cr has very low solubility in Al, but it dissolves to about 3% in Fe at room temperature [28]. This explains the presence of Cr in our Fe-rich precipitates and the absence of any apparent effect of Cr on the mean grain size of the alloys containing Fe.

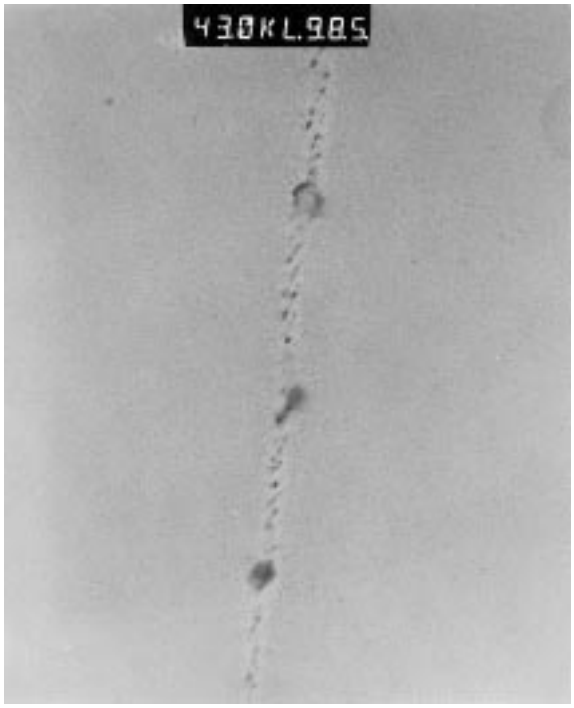

Fig. 4. TEM images of alloy 2B.

3.2. *Electrochemical measurements*

3.2.1. *Open-circuit potential measurements*

Figure 5 shows o.c.p. against time for the alloys immersed in O_2-saturated 0.1 M NaCl. Initially, they increased with time and, after a few minutes, a quasi-steady value was approached. However, the o.c.p.'s showed an oscillation behaviour, the potential changing in a range 15–25 mV around the mean quasisteady value, which was approximately constant, at least for about 5 h. Quasisteady o.c.p. values after 5 h of immersion in O_2-saturated 0.1 M NaCl are shown in Table 2. Each value is the average of three experiments.

SEM observations of the specimens after 5 h of immersion in O_2-saturated 0.1 M NaCl showed pitting attack near the particles containing Fe (Figure 6(a) and (b)), the pits being covered by gel-like precipitates (Figure 6(b)). Corrosion around these particles can be explained, as usual, by the formation of local cells between them (more noble) and the matrix (more active).

O.c.p. values were also obtained following the G69-81 Standard Practice (Figure 7). The form of these curves were interpreted elsewhere [17]. These values, those obtained using O_2-saturated 0.1 M NaCl and previous results corresponding to alloys having the same composition except Fe [17], can be compared in Table 2. Alloy H had the same composition in Mg and Zn as alloy 1, and alloy L, the same composition in Mg, Zn and Cr as alloy 2. As shown in this Table 2, the o.c.p.'s strongly depended on the alloy composition and heat treatment and, therefore, these values can be used to characterize the different alloys.

On the one hand, for all the alloys listed in Table 2, the o.c.p.'s were more negative than those obtained for pure Al in the same media [16]. This is in agreement with previous results [17, 25], which also show that Zn and Mg shift the o.c.p. of Al to more negative potentials and Cr and Cu, to more positive ones. Note that the o.c.p.'s in 1 M NaCl + H_2O_2 are more negative than in O_2-saturated 0.1 M NaCl because of the higher chloride concentration. On the other hand, and as in the case of

Table 2. Quasisteady o.c.p. values measured in O_2-saturated 0.1 M NaCl ($E1$) and following the G69-81 Standard practice [28], i.e. in 1 M NaCl + 9 ml of 30% H_2O_2 per litre ($E2$)

Alloy	$E1$/V	$E2$/V	Alloy	$E1$/V	$E2$/V
1ST	−927	−982	HST*	−860	−966
1A	−960	−976	HA*	−900	−966
1B	−910	−932	HB*	−850	−887
2ST	−860	−935	LST*	−825	−925
2A	−840	−930	LA*	−833	−927
2B	−820	−890	LB*	−825	−860

* Results taken from [17]

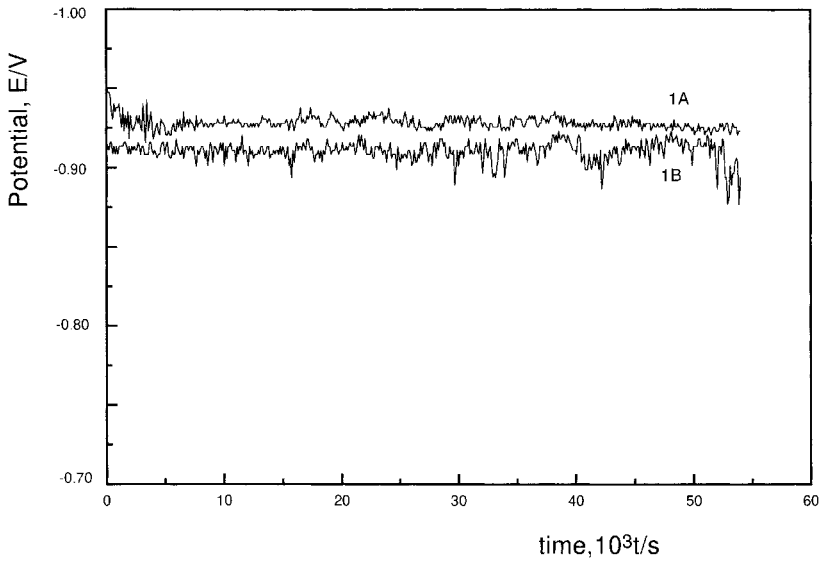

Fig. 5. O.c.p. against time for alloy 1 in O_2-saturated 0.1 M NaCl.

alloys without Fe [17], heat treatment B moved the o.c.p.'s to more positive values.

Table 2 shows that in O_2-saturated 0.1 M NaCl, the presence of Fe causes a negative shift in the o.c.p.'s of about 60 mV (compare alloy 1 with alloy H). However, the o.c.p.'s of alloy 1 in 1 M NaCl + H_2O_2 were only 10–45 mV more negative than for alloy H. Table 2 also shows that Fe produces a smaller shift of the o.c.p.'s of the Cr-containing alloys to more negative values (compare alloy 2 with alloy L), a maximum of 35 mV in O_2-saturated 0.1 M NaCl, and a maximum of 30 mV in 1 M NaCl + H_2O_2.

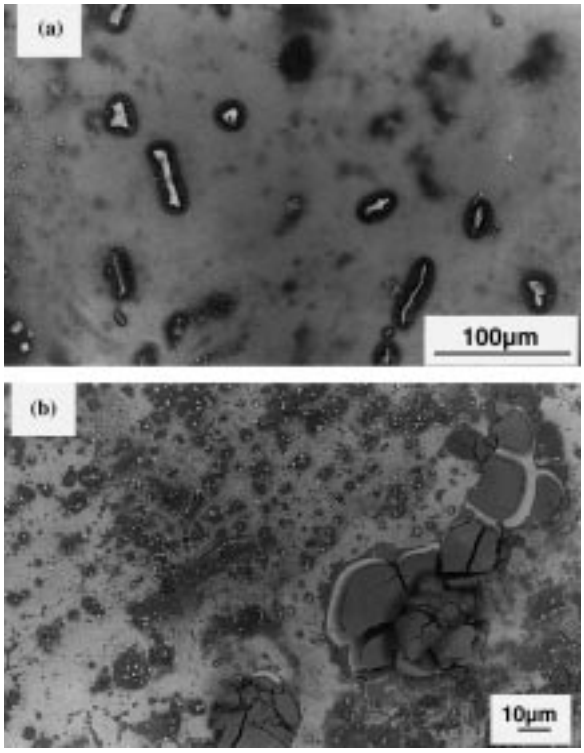

Fig. 6. SEM images of samples 1ST (a) and 1B (b) after immersion in O_2-saturated 0.1 M NaCl.

As Fe has a very low solubility in Al [1], it is present in solid solution at a very small concentration. In addition, the Fe-rich particles have microscopic size. However, small particles of the second phase, formed due to a supersaturation, did not significantly affect the o.c.p.'s of the Al alloys [25]. Nevertheless, Table 2 shows that Fe caused a shift of the o.c.p. in the negative direction. This shift can be explained if we assume a greater amount of Zn and Mg dissolved in the matrix for the Fe-containing alloys (without Cr and also with Cr), that is, Fe limits the $MgZn_2$ growth. This is also in agreement with the smaller amounts of $MgZn_2$ precipitates found in our SEM and TEM observations.

Previous work showed that Cr nuclei behaved as nucleation centres for $MgZn_2$ [17, 29, 30]. As a certain amount of Cr can be found in the Fe-rich particles, less Cr is dispersed in the matrix to accelerate the nucleation of $MgZn_2$ precipitates. This suggests that the amount of Cr is not sufficient to compensate the effect of Fe and explains that the o.c.p.'s of the Cr-containing alloys continue to be somewhat more negative in the presence of Fe. However, some effect of Cr in nucleating the $MgZn_2$ particles exists, with the consequent decrease in the Zn and Mg contents of the Al alloy matrix, because the shift in the o.c.p.'s to more negative values in the presence of Fe is less pronounced for the Cr-containing alloys.

3.2.2. *Cyclic polarization results*

CP curves were obtained in deaerated 0.1 M NaCl, at 1 mV s^{-1}, immediately after the immersion of the alloy in the electrolyte. Typical CP curves for Al–Zn–Mg alloys are shown in Figure 8 Curves of this type were also obtained for Al–5%Zn–1.7%Mg alloys without Fe and were interpreted elsewhere [15, 16, 18, 31]. Specimens submitted to heat treatment B gave cyclic

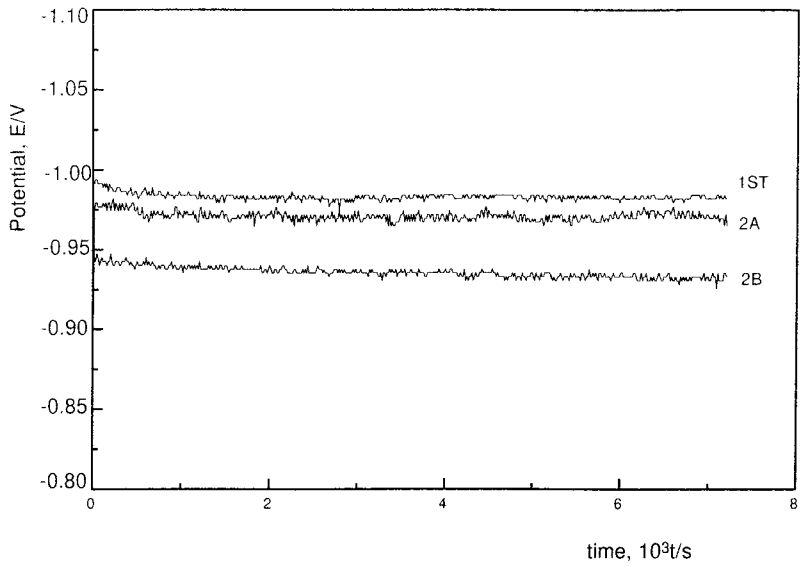

Fig. 7. O.c.p. against time for alloy 1 and 2 in 1.0 M NaCl + H_2O_2 (G 69-81 ASTM Standard Practice).

voltammograms with an anodic maximum before the pit propagation region. Pitting was not observed in the region of the anodic maximum, but a Mg dealloying with oxide growth and dissolution [18, 31]. A small anodic maximum before pitting was also previously found for Al–Fe alloys [24]. In this latter case, however, the anodic maximum was related to the oxidation of Fe present in the intermetallic compounds. In the case of the alloys studied in this work, the anodic maximum cannot be associated with the oxidation of iron because pitting of the aluminium matrix takes place at potentials more negative than that of the Fe oxidation. Therefore, the anodic maxima of specimens 1B and 2B are not due to Fe oxidation, but correspond to the same processes as those found for the Al–Zn–Mg alloys without Fe.

The breakdown (E_{br}) and repassivation (E_{rp}) potentials of alloys 1 and 2 are given in Table 3, where they are compared with those corresponding to the Al–Zn–Mg alloys without Fe (H and L), previously reported [18]. As shown in Table 3 and despite no changes in the form of the cyclic voltammograms of the Al–Zn–Mg alloys in chloride solutions were found, Fe move E_{br} and E_{rp} of the Al–Zn–Mg alloys to more negative potentials.

Table 3. Breakdown (E_{br}) and repassivation (E_{rp}) potentials of Al–Zn–Mg alloys, submitted to heat treatment ST, A and B, measured in deaerated 0.1 M NaCl, $v = 1$ mV s^{-1}

Alloy	E_{br}/mV	E_{rp}/mV	Alloy	E_{br}/mV	E_{rp}/mV
1ST	−885	−920	HST*	−835	−885
1A	−885	−920	HA*	−840	−890
1B	−825	−855	HB*	−740	−815
2ST	−816	−875	LST*	−815	−850
2A	–	–	LA*	−815	−865
2B	−730	−770	LB*	−725	−740

* Results taken from [18]
Standard deviation about 5–10 mV

Thus, the E_{rp} values for alloy 1 were about 30–40 mV more negative than those obtained previously for alloys H. The shifts in the negative direction of the E_{br} values were greater. However, the shifts of E_{br} and E_{rp} of alloy 2 in the same direction were small than those of alloy 1. These results are in agreement with the o.c.p. measurements given in Table 2. This is not surprising because, as shown in Figure 6, oxygen was able to shift the o.c.p.'s towards a potential range in which pitting took place. Therefore, the shift in the E_{br} and E_{rp} values produced by the presence of 0.3% Fe in the alloys can also be explained by the aforementioned effect of Fe in limiting the $MgZn_2$ precipitation (i.e., the Mg and Zn concentrations in the matrix are greater).

Figure 9 shows SEM observations of the samples 1ST and 1B after a positive-going sweep between −1.2 and −0.75 V. According to Figure 8, the pitting corrosion current at the latter potential is higher for alloy 1ST than for alloy 1B and, therefore, pitting attack is more intense in the former. Figure 9 also shows that pitting attack has occurred mainly near the Fe-rich particles. These particles appear then to condition pitting attack near them. This can be explained assuming that a defective oxide film is formed in the surroundings of such Fe-containing particles, thus facilitating the chloride penetration into the oxide film and a further pit nucleation on the alloy.

CP experiments after 3 h of immersion of the samples under open circuit conditions in the O_2-saturated 0.1 M NaCl were also performed. In this case, the breakdown potentials of alloys 1 and 2 were more positive than those listed in Table 3. In addition, the anodic maxima found in the deaerated solution for samples 1B and 2B were missing. These shifts in E_{br} were also found for the Al–Zn–Mg alloys without Fe and were explained by the growth of an aluminium oxide layer because of the oxidation by dissolved O_2 [18].

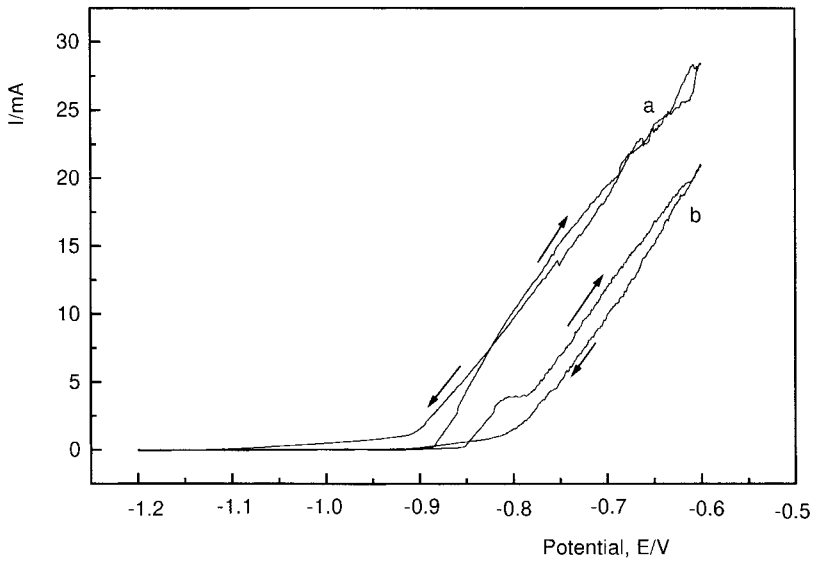

Fig. 8. Polarization curves at 1 mV s^{-1} for samples 1ST (a) and 1B (b), in deaerated 0.1 M NaCl solution.

4. Conclusions

The presence of 0.3% Fe in Al–Zn–Mg alloys produces a significant change in the structure compared to that formed in the absence of Fe. The decrease in the mean grain size by addition of 0.14% Cr is not observed in the presence of Fe. In the Fe-containing Al–Zn–Mg alloys, a large quantity of Fe-rich particles and a small amount of $MgZn_2$ precipitates were observed. EDX microanalysis showed the presence of Cr in the Fe-rich intermetallics.

Open circuit potential measurements in O_2-saturated 0.1 M NaCl or in H_2O_2-containing 1 M NaCl solutions showed that the presence of Fe made the Al–Zn–Mg alloys more anodic and, thus, more susceptible to pitting. This was explained by the existence of less quantity of precipitated $MgZn_2$ in the Fe-containing alloys, corresponding to a greater amount of Zn and Mg in the matrix.

The cyclic polarization curves showed that the presence of Fe in Al–Zn–Mg alloys produced a shift in the breakdown and repassivation potentials to more negative values, in agreement with the results of the o.c.p. measurements. Pitting corrosion mainly occurred near the Fe-rich particles. As Al–Zn–Mg alloys containing Fe were more susceptible to pitting, Fe-free Al should be used as start material to prepare this kind of aluminium-based alloys.

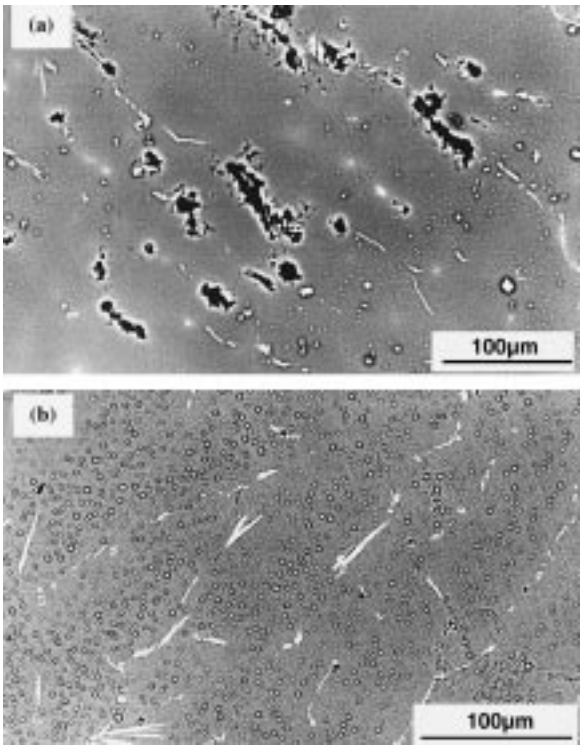

Fig. 9. SEM images of samples 1ST (a) and 1B (b), after a potentiodynamic sweep between −1.2 and −0.75 V at 1 mV s^{-1} in deaerated 0.1 M.

Acknowledgements

The authors gratefully acknowledge the financial support of this work by the CNPq (Proc. 521565/95-2) and the FAPESP, project 95/5230-4. The authors also thank the 'Serveis Científico-Tècnics' of the Universitat de Barcelona for the facilities in the SEM and TEM observations, and the EDX microanalyses.

References

1. L.F. Mondolfo, *Metall. Rev.* **16** (1971) 95.
2. S.C. Byrne, *in* E.A. Stark and T.H. Sanders (Eds), 'Aluminium Alloys, Physical and Mechanical Properties', Vol. 2 (Warley, UK, 1986), pp. 1095–107.
3. C. Blanc, B. Lavele and G. Mankowski, *Corrosion Sci.* **39** (1997) 495.

4. C. Blanc and G. Mankowski, *Corrosion Sci.* **39** (1997) 949.
5. C. Blanc and G. Mankowski, *Corrosion Sci.* **40** (1998) 411.
6. C. Blanc, Y. Roques and G. Mankowski, *Corrosion Sci.* **40** (1998) 1019.
7. S. Maitra and G.C. English, *Metall. Trans.* **12A** (1981) 535.
8. H. Cordier, C. Dumont and W. Gruhl, *Aluminium* **55** (1979) 777.
9. H. Cordier, C. Dumont and W. Gruhl, *Metall.* **34** (1980) 515.
10. H. Cordier, C. Dumont, W. Gruhl and B. Grzembra, *Metall.* **36** (1982) 33.
11. W. Gárlipp, S. Saimoto and H.M. dos Santos, Proceedings of the Meeting of the Associação Brasileira de Metais, Belo Horizonte, Minas Gerais, Brazil (1987), pp. 33–44.
12. I.J. Polmear, *J. Inst. Metals.* **89** (1960–61) 51.
13. M. Cilense, PhD thesis, Instituto de Química, UNESP, Araraquara, Brazil (1990).
14. G. Mankowski, M.L. Perez, J.A. Petit and F. Dabosi, *Corrosion* **40** (1984) 552.
15. A.H. Moreira, PhD thesis, University of Barcelona, Barcelona, Spain (1992).
16. P.L. Cabot, A.H. Moreira, J.A. Garrido, A.V. Benedetti and E. Pérez, *Current Topics in Electrochemistry* **3** (1994) 1–17.
17. P.L. Cabot, J.A. Garrido, E. Pérez, A.H. Moreira, P.T.A. Sumodjo, A.V. Benedetti, *J. Appl. Electrochem.* **25** (1995) 781.
18. J.A. Garrido, P.L. Cabot, A.H. Moreira, R.M. Rodriguez, P.T.A. Sumodjo and E. Pérez, *Electrochim. Acta* **41** (1996) 1933.
19. P.L. Cabot, F. Centellas, J.A. Garrido, E. Pérez, A.H. Moreira, P.T.A. Sumodjo, A.V. Benedetti and W. Proud, *in* 'Progress in the Understanding and Prevention of Corrosion', Vol. 2 (1993), p. 1419. In: J.M. Costa and A.D. Mercer (Eds.), Cambridge.
20. P.L. Cabot, J.A. Garrido, E. Pérez, A.H. Moreira, P.T.A. Sumodjo and W. Proud, *Electrochim. Acta* **40** (1995) 447.
21. L.K. Walford, *Acta Cryst.* **18** (1965) 287.
22. P.J. Black, *Acta Cryst.* **8** (1955) 43.
23. E.H. Hollingsworth, G.R. Jr. Frank, and R.E. Willet, *Trans. Metall. Soc. AIME* **224** (1962) 188.
24. O. Seri and K. Tagashira, *Corrosion Sci* **30** (1990) 87.
25. E.H. Hollingsworth and H.Y. Hunsicker, Corrosion, *in* 'Metals Handbook' (Eds.) 9th edn, Vol. 13 (ASM, Metals Park, OH, 1987), pp. 583–609.
26. R.H. Stevens, Metallography and Microstructures, *in* 'Metals Handbook', 9th edn, Vol. 9 (ASM, Metals Park, OH, 1985), pp. 351–360.
27. ASTM (Ed.) 'Annual Book of ASTM Standards', Vol. 3.02 (ASTM, Philadelphia, 1989), G 69-81, pp. 260–262.
28. T.B. Massalski (Ed-in-chief), 'Binary Alloy Phase Diagrams', 2nd edn, Vols. 1 and 2 (ASM International, USA, 1990).
29. I.J. Polmear, *J. Inst. Metals* **87**, (1958/1959) 65.
30. J.G. Thomas and J. Nutting, *J. Inst. Metals* **88** (1959/1960) 81.
31. J.A. Garrido, P.L. Cabot, R.M. Rodríguez, E. Pérez, A.H. Moreira, P.T.A. Sumodjo and A.V. Benedetti, *J. Appl. Electrochem.* **29** (1999) 1241.